

# Development and use of Kulikovskiy-Sveshnikova-Beghin (KSB) model for avalanches and its application to slide paths of central Montana

Michael Fiore

Director:  
Kelly Cline

Readers:  
Holly Zullo  
Anthony Szpilka

## Abstract


The number of people heading into the backcountry in winter is increasing every year. This increase in travel heightens the risk for human injury due to avalanches, a powerful natural event. The Kulikovskiy-Sveshnikova-Beghin (KSB) avalanche model uses ordinary differential equations for volume, mass, and momentum to model the major characteristics of powder snow avalanches. Although the KSB model has its shortcomings, it provides useful insight into the behavior of avalanches without significant computational cost. The KSB model may predict unrealistically high densities if the snow being entrained is deep and/or high-density. After re-deriving the KSB equations, using Turnbull [4] as a guide, the model will be applied to popular backcountry ski locations in the Helena, MT area. The various slide paths are evaluated using snow conditions observed in the winter of 2013.

SIGNATURE PAGE

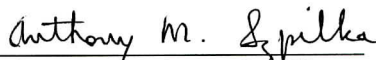
This thesis for honors recognition has been approved for the  
Department of: Math, Engineering, and Computer Science.

  
\_\_\_\_\_  
Director: Dr. Kelly Cline

 4/2/13  
\_\_\_\_\_  
Date

  
\_\_\_\_\_  
Reader: Dr. Holly Zullo

4/2/13  
\_\_\_\_\_  
Date

  
\_\_\_\_\_  
Reader: Dr. Anthony Szpilka

4/2/13  
\_\_\_\_\_  
Date

# Contents

<b>1</b>	<b>Introduction</b>	<b>4</b>
<b>2</b>	<b>KSB Geometry</b>	<b>4</b>
<b>3</b>	<b>Volume</b>	<b>4</b>
<b>4</b>	<b>Buoyancy</b>	<b>7</b>
<b>5</b>	<b>Density</b>	<b>9</b>
<b>6</b>	<b>Momentum</b>	<b>10</b>
<b>7</b>	<b>Velocity</b>	<b>11</b>
<b>8</b>	<b>Analytical Solutions</b>	<b>12</b>
<b>9</b>	<b>Numerical Results</b>	<b>13</b>
9.1	Slope angle as a function of Position . . . . .	14
9.1.1	Data . . . . .	14
9.1.2	Linear . . . . .	15
9.1.3	Sinusoidal . . . . .	15
9.1.4	Linear and Sinusoidal . . . . .	16
9.1.5	Linear with Position Dependent Sinusoidal . . . . .	17
9.1.6	Choosing a Model . . . . .	18
9.2	Step Size . . . . .	18
9.3	Copper Bowls Results . . . . .	18
9.4	Stonewall Results . . . . .	21
9.5	Morrell Results . . . . .	22
<b>10</b>	<b>Strengths and Weaknesses</b>	<b>23</b>
<b>11</b>	<b>Future Possibilities</b>	<b>25</b>
<b>12</b>	<b>Conclusion</b>	<b>25</b>

# 1 Introduction

The rapid growth of the outdoor industry has drastically increased the number of people heading into the backcountry during the winter months. This increase in backcountry travel heightens the risk for human triggered avalanches.

An avalanche is defined as “a large mass of snow, ice etc., detached from a mountain slope and sliding or falling suddenly downward”[1]. Avalanches usually occur on interfaces in the snowpack; backcountry travelers often refer to these interfaces as weak layers. These weak layers tend to happen at three distinct locations within the snow pack: the interface between older snow and new snowfall, on sun or rain crusts, or at hoar frost layers. Weak layers usually heal over time; however, the length of the process varies significantly based on the moisture content of the snow, temperature, wind and a variety of other factors. By analyzing these weak layers, it is possible to predict at what depth the avalanche may trigger.

Human triggered avalanches occur mostly on slopes between 32 and 46 degrees. This avalanche “sweet” spot exists because the snow on lower angle slopes does not hold enough energy to create a sustained downward slide, and avalanches on slopes above 46 degrees are unlikely because on these very steep slopes, natural avalanches occur frequently, making a significant, human triggered avalanche unlikely.

This paper will analyze the Kulikovkiy-Sveshnikova-Beghin (KSB) model for avalanches. The KSB model uses equations for volume, mass, and momentum to analyze the main characteristics of the avalanche. Then, the model will be adapted for a few of the most likely slide paths frequented by people in the Helena, MT area. For this analysis, the data was gathered during the winter months of 2013 in order to analyze how sizable the avalanches on these slopes would be based on current snow conditions.

## 2 KSB Geometry

The KSB model represents the powder cloud of the avalanche as a half-ellipse with length  $l$  and height  $h$  moving down a slope of angle  $\theta$  with center of mass velocity  $u$  and front velocity  $u_f$  (see Figure 1). As the avalanche moves downslope, it takes in or entrains more snow. The entrainment depth is usually the same as the depth of the weak layers discussed earlier and is represented by  $h_n$ . The density of the snow being entrained  $\rho_s$  greatly affects the avalanche’s characteristics. During its life, the avalanche not only entrains snow, but also takes in air. For this reason it is also important to include the density of air,  $\rho_a$  in the model.

## 3 Volume

The volume will change throughout the life of an avalanche. A volume equation for the avalanche can be derived by assuming the volume occupied by the entrained snow is small compared to the volume occupied by the entrained air [4]. Looking at the geometry of the KSB model, the volume will depend on the height of the powder cloud, the length of the powder cloud, the entrainment depth, and the velocity. The

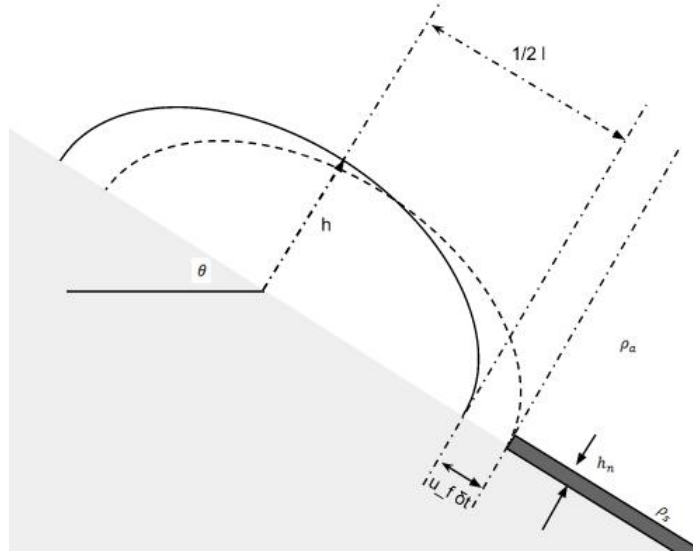


Figure 1: The dashed ellipse represents the avalanche after a time  $\delta t$

height of the powder cloud will be a function of distance downslope from the trigger point ( $s$ ), and some function of the Richardson Number ( $f(Ri)$ ) [4]. The Richardson Number is defined to be the ratio of potential energy to kinetic energy[6]. This gives us the equation  $h = sf(Ri)$ ; however, the height of the powder cloud varies over time. This is represented by:

$$\frac{dh}{dt} = \frac{ds}{dt} f(Ri)$$

which can be rewritten as:

$$\frac{dh}{dt} = uf(Ri)[4]$$

The volume of the cloud will depend on the entrainment coefficient  $\alpha_\nu$ , which describes how much air is being drawn into the avalanche, and is also a function of the Richardson Number and the velocity  $u$ . This leads us to the equation  $\alpha_\nu = f(Ri)\sqrt{\frac{\pi}{k}}$ [4], where  $k$  is the ratio of  $h$  to  $l$ . Therefore the change in volume with respect to time per one meter width will be represented as:

$$\frac{dV}{dt} = \frac{dh}{dt} l$$

We then substitute the change in height equation from above and  $\alpha_\nu$ . The height  $h$  and  $l$  are proportional to the  $\sqrt{V}$  for the elliptical geometry:

$$\frac{dV}{dt} = \alpha_\nu u \sqrt{V}$$

For the analytical solutions the equation is non-dimensionalized such that:

$$(\tilde{s}, \tilde{\rho}_a, \tilde{u}) = \left( \frac{s}{L}, \frac{\rho_a}{\rho_s}, \frac{u}{\sqrt{Lg}} \right)$$

With  $L$  being some arbitrary length scale, and  $g$  the acceleration due to gravity. This leaves the non-dimensional volume equation to be:

$$\frac{d\tilde{V}}{dt} = \alpha_\nu \tilde{u} \sqrt{\tilde{V}}$$

Due to the difficulty of determining exactly where the slide path will end and where points of interest are with respect to time, it would prove more useful to have the volume equation dependent on position. This results in the following:

$$\begin{aligned} \frac{d\tilde{V}}{dt} &= \alpha_\nu \tilde{u} \sqrt{\tilde{V}} \\ \frac{d\tilde{V}}{dt} &= \alpha_\nu \frac{d\tilde{s}}{dt} \sqrt{\tilde{V}} \\ \frac{d\tilde{V}}{d\tilde{s}} &= \alpha_\nu \sqrt{\tilde{V}} \\ 2 \frac{d}{d\tilde{s}} \sqrt{\tilde{V}} &= \alpha_\nu \end{aligned}$$

In order to get volume strictly as a function of position, we must integrate this equation:

$$\begin{aligned} \int 2d\sqrt{\tilde{V}} &= \int \alpha_\nu d\tilde{s} \\ 2\sqrt{\tilde{V}} &= \int \alpha_\nu d\tilde{s} \\ 4\tilde{V} &= \left[ \int \alpha_\nu d\tilde{s} \right]^2 \end{aligned}$$

Next, we integrate from the virtual origin  $\tilde{s}_{sov}$  to  $\tilde{s}$

Assuming the entrainment of ambient air is constant, i.e.  $\alpha_\nu$  is constant, the integral becomes trivial.

This leaves us with:

$$\tilde{V} = \left[ \frac{\alpha_\nu (\tilde{s} - \tilde{s}_{sov})}{2} \right]^2$$

## 4 Buoyancy

In the KSB model, the buoyancy of the powder cloud is defined to be the relative density of the cloud to the fluid surrounding it. The resulting buoyancy equation is:

$$B = \rho V - \rho_a V$$

where  $\rho$  is the density of the avalanche,  $\rho_a$ , the density of air, and  $V$  the volume of the avalanche. This implies that  $\rho V$  is the full mass of the avalanche, which could be rewritten as the sum of the mass of entrained snow,  $m_s$ , and the mass of entrained air,  $m_a$ . Therefore the buoyancy equation becomes:

$$B = m_s + m_a - \rho_a V$$

The change in volume with respect to time can be thought of as the volume flux of air into the cloud from its surroundings, added to the volume flux of snow which is being entrained from the bottom surface of the avalanche:

$$\frac{dV}{dt} = q_a + q_s$$

We can use this equation for change in volume to find the change in mass with respect to time:

$$\frac{dm_s}{dt} = \rho_s q_s, \quad \frac{dm_a}{dt} = \rho_a q_a$$

We then differentiate the buoyancy equation and substitute the derivative for  $m_s$  and  $m_a$ :

$$\begin{aligned} B &= m_s + m_a - \rho_a V \\ \frac{dB}{dt} &= \frac{dm_s}{dt} + \frac{dm_a}{dt} - \rho_a \frac{dV}{dt} \\ \frac{dB}{dt} &= \rho_s q_s + \rho_a q_a - \rho_a (q_a + q_s) \\ \frac{dB}{dt} &= q_s (\rho_s - \rho_a) \end{aligned}$$

The value of  $q_s$  can be expressed in terms of the depth of the snow being entrained, or the erosion depth. We will use  $h_n$  to express this value. Recall, the erosion depth is usually determined by the natural layers within a snow pack. The avalanche will slide on top of one of these naturally occurring layers. In this 2D model, the erosion depth multiplied by the front velocity will give the flux of snow into the avalanche per unit width. Therefore the buoyancy equation becomes:

$$\frac{dB}{dt} = u_f h_n (\rho_s - \rho_a)$$

In order to reduce the number of variables, we will find the equation for  $u_f$  in terms of the center of mass velocity, using the geometry of the semiellipse:

$$u_f = u + \frac{1}{2} \frac{dl}{dt}. \tag{1}$$

We must now find the equation of  $\frac{1}{2} \frac{dl}{dt}$ . Because  $l$  is primarily involved in the volume equation, we begin with the volume equation, and must find how it changes with time:

$$V = \frac{1}{4} \pi h l$$

Taking the derivative of volume with respect to time:

$$\frac{dV}{dt} = \frac{\pi}{4} \left( h \frac{dl}{dt} + l \frac{dh}{dt} \right)$$

then substituting  $\frac{dV}{dt}$  and  $\frac{dh}{dt}$  from above:

$$\alpha_\nu u \sqrt{V} = \frac{\pi}{4} \left( h \frac{dl}{dt} + l u f(Ri) \right)$$

and substitute the equation of the Richardson Number:

$$\alpha_\nu u \sqrt{V} = \frac{\pi}{4} \left( h \frac{dl}{dt} + l u \alpha_\nu \sqrt{\frac{k}{\pi}} \right)$$

$$\begin{aligned} \frac{\alpha_\nu u \sqrt{V}}{\pi h} &= \frac{1}{4} \frac{dl}{dt} + \frac{l u \alpha_\nu \sqrt{k \pi}}{4 \pi h} \\ \frac{\alpha_\nu u \sqrt{V}}{\pi h} - \frac{l u \alpha_\nu \sqrt{k \pi}}{4 \pi h} &= \frac{1}{4} \frac{dl}{dt} \\ \frac{2 \alpha_\nu u \sqrt{V}}{\pi h} - \frac{l u \alpha_\nu \sqrt{k \pi}}{2 \pi h} &= \frac{1}{2} \frac{dl}{dt} \end{aligned}$$

substitute the equation for V

$$\begin{aligned} \frac{2 \alpha_\nu u \sqrt{\frac{1}{4} \pi h l}}{\pi h} - \frac{l u \alpha_\nu \sqrt{\frac{h}{l} \pi}}{2 \pi h} &= \frac{1}{2} \frac{dl}{dt} \\ \frac{\alpha_\nu u \sqrt{l}}{\sqrt{\pi h}} - \frac{\alpha_\nu u \sqrt{l}}{2 \sqrt{\pi h}} &= \\ \frac{\alpha_\nu u}{2 \sqrt{\pi k}} &= \frac{1}{2} \frac{dl}{dt} \end{aligned}$$

We can now substitute this new equation for  $\frac{1}{2} \frac{dl}{dt}$  back into our original equation (1) for  $u_f$ :

$$u_f = u \left( 1 + \frac{\alpha_\nu}{2 \sqrt{\pi k}} \right) \quad (2)$$

We can now substitute this equation for  $u_f$  back into our buoyancy equation. This now gives us the buoyancy in terms of clearly defined variables:

$$\frac{dB}{dt} = (\rho_s - \rho_a) \cdot h_n u \left( 1 + \frac{\alpha_\nu}{2\sqrt{\pi k}} \right)$$

Similar to the volume equation, buoyancy would be more useful if it were spatially dependent instead of time dependent.

Thus we convert buoyancy to a spatial derivative:

$$\frac{dB}{dt} = (\rho_s - \rho_a) \cdot h_n u \left( 1 + \frac{\alpha_\nu}{2\sqrt{\pi k}} \right)$$

This can be rewritten as:

$$\begin{aligned} \frac{dB}{dt} &= (\rho_s - \rho_a) \cdot h_n \frac{ds}{dt} \left( 1 + \frac{\alpha_\nu}{2\sqrt{\pi k}} \right) \\ \frac{\frac{dB}{dt}}{\frac{ds}{dt}} &= (\rho_s - \rho_a) \cdot h_n \left( 1 + \frac{\alpha_\nu}{2\sqrt{\pi k}} \right) \\ \frac{dB}{ds} &= (\rho_s - \rho_a) \cdot h_n \left( 1 + \frac{\alpha_\nu}{2\sqrt{\pi k}} \right) \end{aligned}$$

When this is non-dimensionalized we obtain:

$$\frac{d\tilde{B}}{d\tilde{s}} = (1 - \tilde{\rho}_a) \cdot \tilde{h}_n \left( 1 + \frac{\alpha_\nu}{2\sqrt{\pi k}} \right)$$

To make the equation simpler, we define  $\eta = (1 - \tilde{\rho}_a) \cdot \tilde{h}_n \left( 1 + \frac{\alpha_\nu}{2\sqrt{\pi k}} \right)$ , The buoyancy equation then becomes:

$$\tilde{B} = \int_{\tilde{s}_{ob}}^{\tilde{s}} \eta(\tilde{s}') d\tilde{s}' \quad (3)$$

## 5 Density

In order to find the density, we must refer to how we defined buoyancy earlier:  $\tilde{B} = (\tilde{\rho} - \tilde{\rho}_a) \tilde{V}$ . By assuming  $\eta$  to be constant we can integrate buoyancy directly. The buoyancy equation becomes:  $\tilde{B} = \eta(\tilde{s} - \tilde{s}_{ob})$ . By substituting this buoyancy equation, as well as the volume equation from above, the equation for density becomes:

$$\tilde{\rho} = \frac{4\eta(\tilde{s} - \tilde{s}_{ob})}{\alpha_\nu^2(\tilde{s} - \tilde{s}_{ov})^2} + \tilde{\rho}_a \quad (4)$$

## 6 Momentum

The force created by the avalanche can be found by using the definitions of force and momentum:

$$F = ma$$

$$F = \frac{dp}{dt} = ma$$

$$\frac{d}{dt}(M \cdot u) = Bg\sin(\theta)$$

We now use  $\chi$  as the added mass coefficient[4]. The mass of the avalanche can be found to be:

$$M = B + (1 + \chi)V\rho_a [4]$$

The force equation nondimensionalized becomes:  $\frac{d}{dt}(\tilde{M} \cdot \tilde{u}) = \tilde{B}\sin(\theta)$ . An energy equation can be found by multiplying both sides of the momentum equation by  $\tilde{M}$ [4]:

$$\tilde{M} \frac{d}{dt}(\tilde{M} \cdot \tilde{u}) = \tilde{M}\tilde{B}\sin(\theta)$$

We must next convert the time derivative to a spatial derivative:

$$\tilde{M} \left( \frac{d\tilde{M}}{dt} \cdot \tilde{u} + \tilde{M} \cdot \frac{d\tilde{u}}{dt} \right) = \tilde{M}\tilde{B}\sin(\theta)$$

We then divide both sides by velocity:

$$\tilde{M} \frac{\left( \frac{d\tilde{M}}{dt} \cdot \tilde{u} + \tilde{M} \cdot \frac{d\tilde{u}}{dt} \right)}{\tilde{u}} = \frac{\tilde{M}\tilde{B}\sin(\theta)}{\tilde{u}}$$

$$\tilde{M} \frac{\left( \frac{d\tilde{M}}{dt} \cdot \tilde{u} + \tilde{M} \cdot \frac{d\tilde{u}}{dt} \right)}{\frac{d\tilde{s}}{dt}} = \frac{\tilde{M}\tilde{B}\sin(\theta)}{\tilde{u}}$$

$$\tilde{M} \left( \frac{d\tilde{M}}{dt} \cdot \frac{dt}{d\tilde{s}} \cdot \tilde{u} + \tilde{M} \cdot \frac{d\tilde{u}}{dt} \cdot \frac{dt}{d\tilde{s}} \right) = \frac{\tilde{M}\tilde{B}\sin(\theta)}{\tilde{u}}$$

$$\tilde{u}\tilde{M} \left( \frac{d\tilde{M}}{d\tilde{s}} \cdot \tilde{u} + \tilde{M} \cdot \frac{d\tilde{u}}{d\tilde{s}} \right) = \tilde{M}\tilde{B}\sin(\theta)$$

$$\tilde{u}\tilde{M} \frac{d}{d\tilde{s}}(\tilde{u}\tilde{M}) = \tilde{M}\tilde{B}\sin(\theta)$$

This can be simplified to:

$$\frac{1}{2} \frac{d}{d\tilde{s}}(\tilde{u}\tilde{M})^2 = \tilde{M}\tilde{B}\sin(\theta)$$

We must then solve this so we have the equation for velocity as a function of position:

$$\tilde{u} = \frac{1}{\tilde{M}} \sqrt{2 \int_{\tilde{s}_{ou}}^{\tilde{s}} \tilde{M} \tilde{B} \sin \theta ds} \quad (5)$$

Remember:  $\theta$ ,  $\tilde{M}$ , and  $\tilde{B}$  are all functions of position.

## 7 Velocity

For the analytical solutions for the velocity equation, we assume  $\theta$ ,  $\tilde{M}$ , and  $\tilde{B}$  are all constant. This allows us to integrate the velocity function explicitly:

$$\tilde{u} = \frac{1}{\tilde{M}} \sqrt{2 \int_{\tilde{s}_{ou}}^{\tilde{s}} \tilde{M} \tilde{B} \sin \theta d\tilde{s}}$$

Substituting the equations for mass and buoyancy results in:

$$\tilde{u} = \frac{1}{\tilde{M}} \sqrt{2 \int_{\tilde{s}_{ou}}^{\tilde{s}} [B + (1 + \chi)V\rho_a] \tilde{B} \sin \theta d\tilde{s}}$$

To clean up the equation, we let  $\beta = (1 + \chi)\rho_a$ . This leads us to the equation:

$$\tilde{u} = \frac{1}{\tilde{M}} \sqrt{2 \int_{\tilde{s}_{ou}}^{\tilde{s}} (B + \beta V) \tilde{B} \sin \theta d\tilde{s}}$$

$$\tilde{u} = \frac{1}{\tilde{M}} \sqrt{2 \int_{\tilde{s}_{ou}}^{\tilde{s}} \left[ \left( \int_{\tilde{s}_{oB}}^{\tilde{s}} \eta d\tilde{s}' + \beta \frac{1}{4} [\alpha_\nu (\tilde{s} - \tilde{s}_{ov})]^2 \right) \int_{\tilde{s}_{oB}}^{\tilde{s}} \eta d\tilde{s}' \sin \theta \right] d\tilde{s}}$$

$$\tilde{u} = \frac{1}{\tilde{M}} \sqrt{2 \int_{\tilde{s}_{ou}}^{\tilde{s}} \left[ \left( \eta (\tilde{s} - \tilde{s}_{oB}) + \beta \frac{1}{4} [\alpha_\nu (\tilde{s} - \tilde{s}_{ov})]^2 \right) \eta (\tilde{s} - \tilde{s}_{oB}) \sin \theta \right] d\tilde{s}}$$

$$\tilde{u} = \frac{1}{\tilde{M}} \sqrt{2\eta^2 \sin \theta \int_{\tilde{s}_{ou}}^{\tilde{s}} (\tilde{s} - \tilde{s}_{oB})^2 d\tilde{s} + \frac{1}{2} \beta \sin \theta \int_{\tilde{s}_{ou}}^{\tilde{s}} [\alpha_\nu (\tilde{s} - \tilde{s}_{ov})]^2 \eta (\tilde{s} - \tilde{s}_{oB}) d\tilde{s}}$$

$$\tilde{u} = \frac{1}{\tilde{M}} \sqrt{2\eta^2 \sin\theta \left[ \frac{1}{3}\tilde{s}^3 - \tilde{s}_{oB}\tilde{s}^2 + \tilde{s}\tilde{s}_{oB}^2 \Big|_{\tilde{s}_{ou}}^{\tilde{s}} \right] + \frac{1}{2}\beta\alpha_\nu^2 \eta \sin\theta \left[ \tilde{s}^2 \cdot \left( \frac{1}{2}\tilde{s}_{ov}^2 + \tilde{s}_{oB} \cdot \tilde{s}_{ov} \right) - \tilde{s}^3 \cdot \left( \frac{1}{3}\tilde{s}_{oB} + \left( \frac{2}{3} \cdot \tilde{s}_{ov} \right) \right) + \frac{1}{4}\tilde{s}^4 - \tilde{s} \cdot \tilde{s}_{oB} \cdot \tilde{s}_{ov}^2 \right] \Big|_{\tilde{s}_{ou}}^{\tilde{s}}}$$

To simplify the equation we choose our virtual origin  $\tilde{s}_{ou} = 0$ . We now define  $f(s)$  to be:

$$f(\tilde{s}) = 2\eta \left[ \frac{1}{3}\tilde{s}^2 - \tilde{s}_{oB}\tilde{s} + \tilde{s}_{oB}^2 \right] + \frac{1}{2}\beta\alpha_\nu^2 \left[ \tilde{s} \cdot \left( \frac{1}{2}\tilde{s}_{ov}^2 + \tilde{s}_{oB} \cdot \tilde{s}_{ov} \right) - \tilde{s}^2 \cdot \left( \frac{1}{3}\tilde{s}_{oB} + \frac{2}{3} \cdot \tilde{s}_{ov} \right) + \frac{1}{4}\tilde{s}^3 - \tilde{s}_{oB} \cdot \tilde{s}_{ov}^2 \right]$$

This now leaves us with the velocity equation:

$$\tilde{u} = \frac{\sqrt{\eta \tilde{s} f(\tilde{s}) \sin(\theta)}}{\tilde{M}} \quad (6)$$

## 8 Analytical Solutions

Using the initial conditions given in Turnbull [4], we created graphs of density and velocity versus time. In order to more accurately view how the characteristics of the avalanche are changing over time, we chose our arbitrary length scale, L, to be 4. We used the following values:

$$\begin{aligned} V_0 &= 10m^3 \\ \rho_0 &= 100 \frac{Kg}{m^3} \\ h_n &= 0.4m \\ \rho_s &= 150 \frac{Kg}{m^3} \\ \rho_a &= 1.04 \frac{Kg}{m^3} \\ k &= 0.4 \\ \chi &= .4 \\ \theta &= 30 \end{aligned}$$

Using these initial conditions, we plotted density and velocity for three values of  $\alpha_\nu$ , .05, .1, and .5 also gathered from Turnbull [2007]. See Figure 2. The higher the entrainment coefficient, the faster the avalanche reaches its maximum velocity; however, the maximum velocity is also lower as the entrainment coefficient continues to grow.

As the avalanche moves downhill, it experiences a rise in density; however, as it begins to move faster and take in more of the ambient air which is surrounding it, it begins to lose density and approaches the density of air near the end of the slide path. It is important to remember the KSB model does not account for the settling process at the end of the avalanche. The density is shown in Figure 3

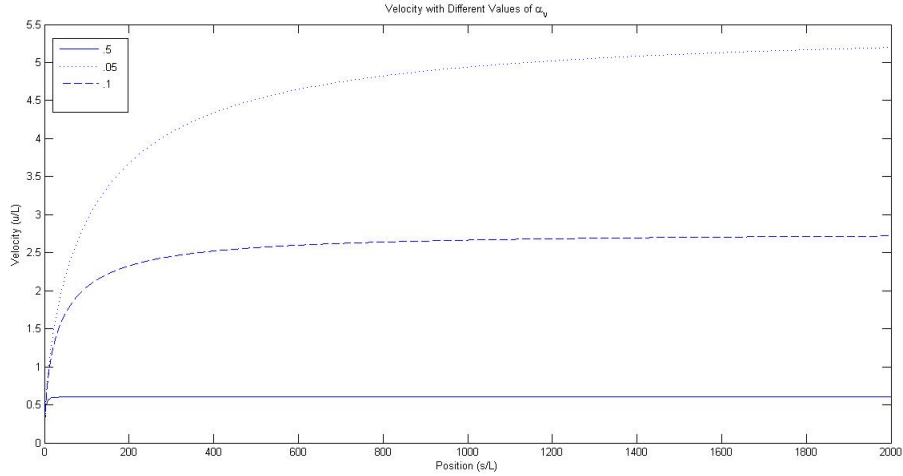


Figure 2: Graph of velocity for  $\alpha_\nu = .05$ , dotted line,  $\alpha_\nu = .1$ , dashed line, and  $\alpha_\nu = .5$ , solid line.

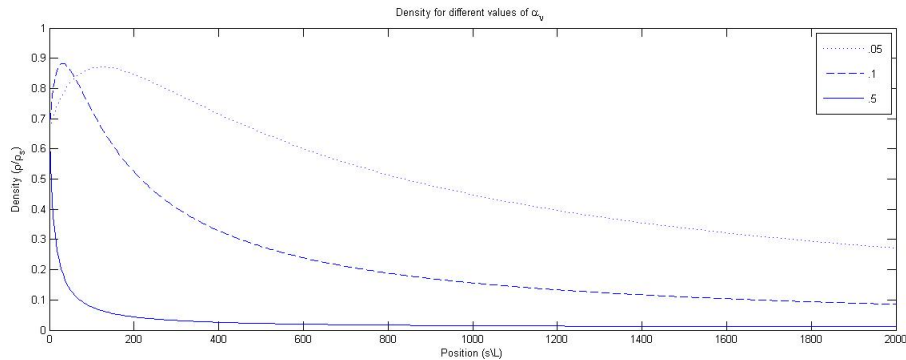


Figure 3: Graph of density for  $\alpha_\nu = .05$ , dotted line.  $\alpha_\nu = .1$ , dashed line, and  $\alpha_\nu = .5$ , solid line.

## 9 Numerical Results

In order for the KSB equations to be solved analytically, we had to make some significant simplifying assumptions that are not representative of real life situations, such as constant entrainment coefficients and a constant Richardson Number. In order to avoid some of these assumptions, we chose to integrate the differential equation numerically using Euler's Method. In order to do this, we must first find the equations for the non-constant terms. The equations for the Richardson Number,  $\alpha_\nu$ ,  $h$ , and  $k$  are taken from Turnbull [4]:

$$\text{Ri} = \frac{(\rho - \rho_a)gh\cos\theta}{\rho_a u^2} \quad (7)$$

$$h = 2\sqrt{\frac{kV}{\pi}} \quad (8)$$

$$\alpha_\nu = \begin{cases} e^{-\lambda Ri^2}, & Ri \leq 1, \\ \frac{e^{-\lambda}}{Ri}, & Ri > 1 \end{cases} \quad (9)$$

$$k = (.002155 + .0732 \cdot \theta)^3 \quad (10)$$

However, for our cases, the Richardson Number is always greater than one so the first piece of equation 9 can be neglected.

## 9.1 Slope angle as a function of Position

### 9.1.1 Data

For this analysis, we gathered our data from Google Earth. To verify that this data is correct we went on several trips and took fifteen manual measurements of slope angle and compared these measurements to those gathered from Google Earth. We found only a one to two degree difference between the measurements. With only these minimal discrepancies, we were able to use the data gathered from Google Earth without introducing large uncertainties.

After this initial analysis, we used Google Earth to map the path an avalanche would most likely follow. Once this path was mapped, we used the elevation profile, which also contains the percent grade, to gather our data. We recorded the measurements of percent grade every five meters over the length of the projected path. Once all of this was entered into Excel (2010), we converted the percent grade to angles in degrees using the formula:

$$\theta = \arctan \left( \frac{\text{Percent Grade}}{100} \right) \quad (11)$$

This gave us the graph in Figure 4.

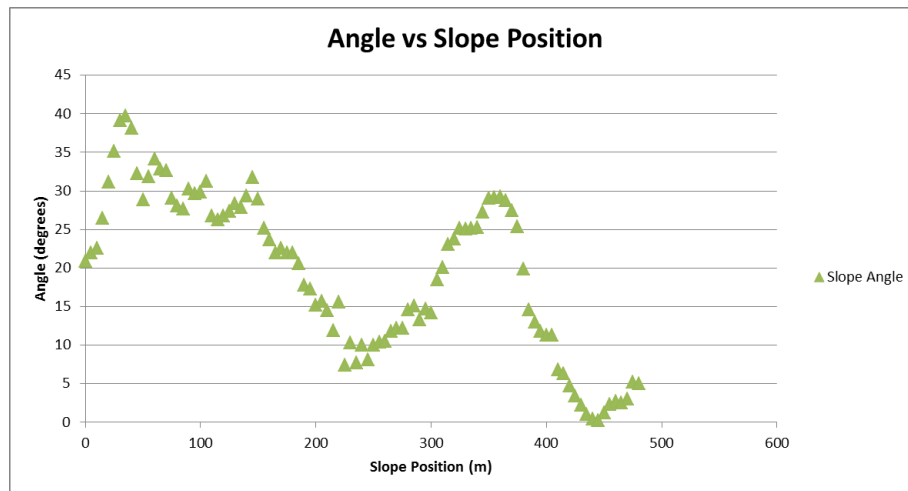


Figure 4: Slope Angle vs. Slope Position

After looking at the graph of the data, it is not immediately obvious which type of regression will fit this data set best.

### 9.1.2 Linear

Although the data does not appear to follow a linear trend, it is important to see if there is some underlying linearity. For this initial model, the standard linear form was used:

$$y = A \cdot x + B \quad (12)$$

Looking at the graph, the y-intercept was estimated to be approximately thirty. Excel Solver (2010) found the solution  $A = -0.05390$ ,  $B = 32.39$  with the sum of the squares of the residuals to be 4801. A graph of the model and the data is shown in Figure 5.

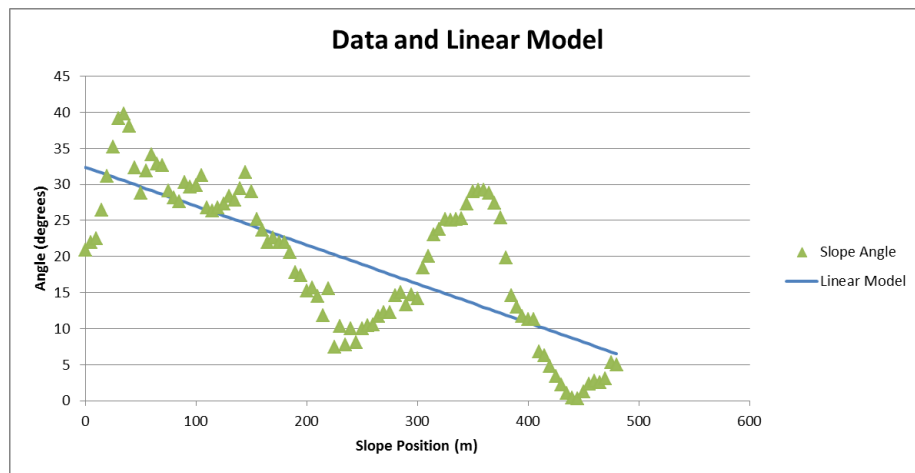


Figure 5: Graph of Data and Linear Model

Upon analyzing the fit of this model, it is obvious there is still work to be done. However, this model does highlight a negative linear trend that was not apparent in the initial examination.

### 9.1.3 Sinusoidal

The next logical choice of model is a sinusoidal model because the graph of the data shows significant resemblance to some sort of oscillating function. For this next model, we used the general form for sinusoidal waves:

$$A \sin(B \cdot x + C) + D \quad (13)$$

We estimated the data to have its first peak at roughly 75m and a second at 350m. Using this information angular frequency is  $\frac{2 \cdot \pi}{350 - 75} \approx .0228$ . After seeing how well this estimate fit the data, we used the Solver.

Solver found the solution to be:

$$\begin{aligned}A &= 10.51 \\B &= 0.02458 \\C &= -0.4121 \\D &= 19.05\end{aligned}$$

This model has a sum of the squares of the residuals of 4985. This model appears

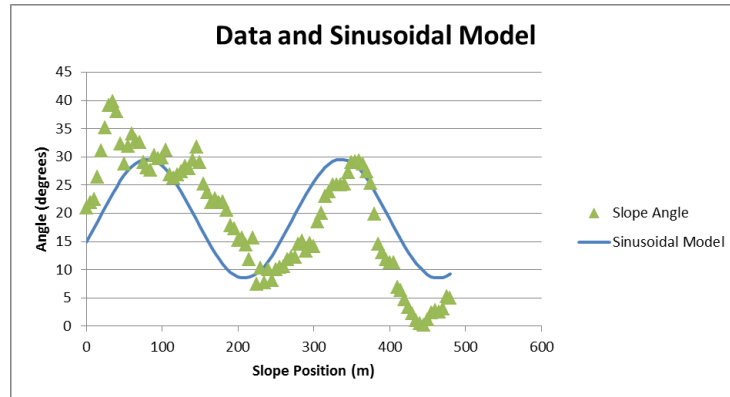


Figure 6: Graph of Data and Sinusoidal Model

to follow the general trend of the data; however, it has a slightly higher sum of the squares of the residuals.

#### 9.1.4 Linear and Sinusoidal

The data exhibits a linearly decreasing trend as well as oscillatory behavior; this leads to the combination of the previous two models, and takes the form:

$$Ax + B\sin(C \cdot x + D) + E \tag{14}$$

Solver gave the solution:

$$\begin{aligned}A &= -0.04610 \\B &= 8.378 \\C &= 0.02483 \\D &= 3.930 \\E &= 30.19\end{aligned}$$

With a sum of the squares of the residuals of 1607, this is a significant improvement over the models when analyzed independently. Results from this model are shown in Figure 7

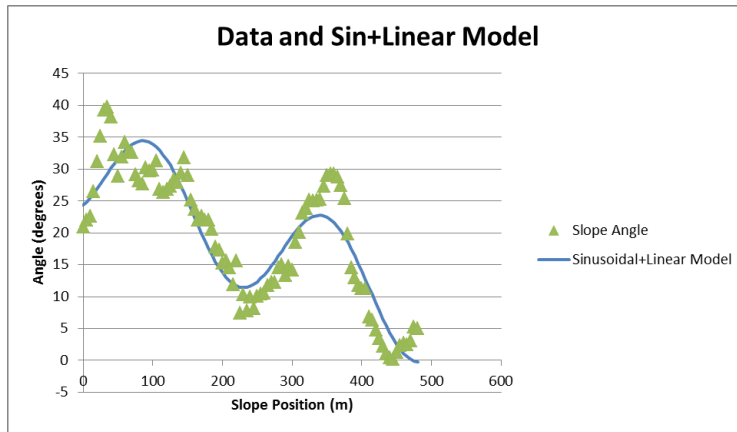


Figure 7: Graph of Data with Sinusoidal and Linear combination Model

### 9.1.5 Linear with Position Dependent Sinusoidal

After more closely examining our data we considered the amplitude may be changing. We then factored in a position dependent amplitude to our sine function. This yielded the general equation:

$$Ax + B \cdot x \sin(C \cdot x + D) + E \quad (15)$$

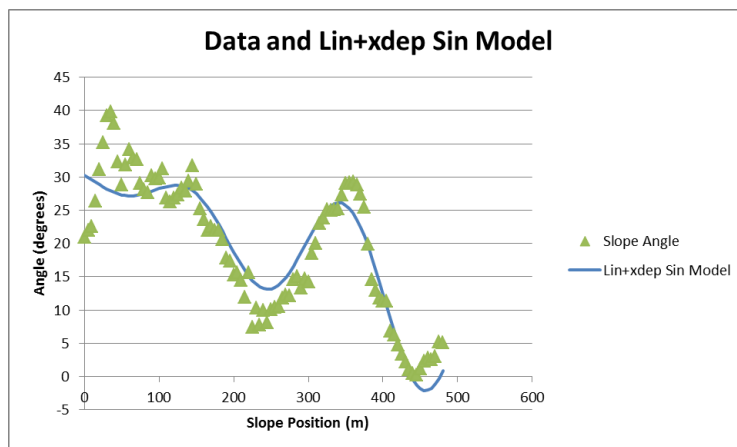


Figure 8: Graph of Data and Linear added to a position dependent sinusoidal function

Solver gave the solution:

$$A = -0.04183$$

$$B = 0.02960$$

$$C = 0.02905$$

$$D = 2.614$$

$$E = 30.28$$

with a sum of the squares of the residuals of 1528. This is shown in Figure 8

### 9.1.6 Choosing a Model

The combination of the sinusoidal and linear model fits our data the best. Although this model does not have the smallest sum of the squares of the residuals, the  $x$  dependent sinusoidal function did not match the qualitative aspects of our data. For example the  $x$  dependent amplitude sinusoidal model was missing the first peak. The linearly decreasing sinusoidal model would not be useful for extrapolation because once the main ski slope is over the landscape significantly changes. Or, in other words, at the end of the run the terrain gets flat and the slope angle would diminish to zero whereas our model predicts the terrain would begin to go uphill. For modeling avalanche paths extrapolation is not going to be important because we know from general avalanche behavior that the avalanche will not continue once the slope angle has decreased to near zero.

However, for interpolation this model is fairly accurate; it incorporates the major qualitative attributes of the graph and has a fairly small sum of the squares of the residuals. For example, the model and the data start with an increase in slope angle and then decrease before having another increase in slope angle after which both the model and data decrease to nearly zero.

## 9.2 Step Size

Using Euler's Method, we were able to integrate the equations for volume density and velocity numerically. We used the same initial conditions with different step sizes in order to ensure we were getting real results and not just numerical "noise." The graphs of velocity, density, and volume are contained in Figures 9, 10, and 11, respectively, for step sizes of .01m, .02m, and .5m. The graphs of each characteristic are virtually indistinguishable from each other. Therefore, we can conclude that Euler's Method with step size .5m will produce accurate enough results for this analysis.

## 9.3 Copper Bowls Results

Using data gathered in the field, we are able to see what the characteristics of the avalanche would be for certain days of backcountry skiing. Throughout the course of the season in the Lincoln area, we found a weak layer at 18cm with the surface

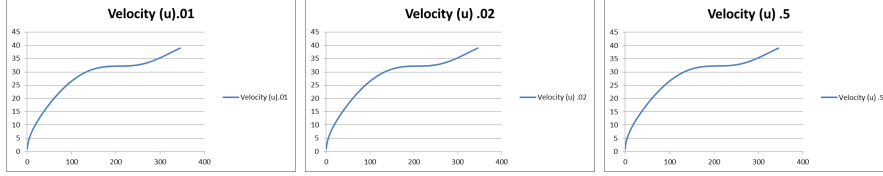


Figure 9: Graphs of velocity for step size .01m, .02m, and .5m respectively

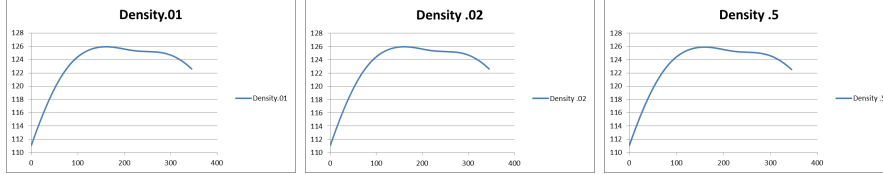


Figure 10: Graphs of density for step size .01m, .02m, and .5m respectively

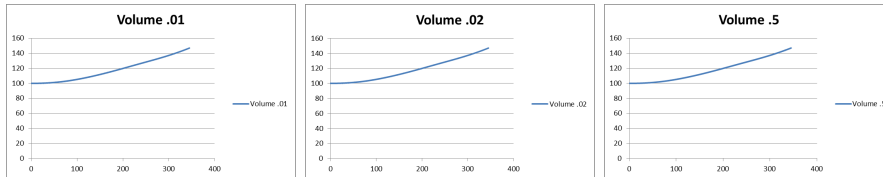


Figure 11: Graphs of volume for step size .01m, .02m, and .5m respectively

snow at 11% water giving it a density of  $110 \frac{Kg}{m^3}$ . There was also another weak layer at 28 cm down with the snow right above that layer at 16% water, giving it a density of  $160 \frac{Kg}{m^3}$ . The final layer of concern is located at 55 cm and had a snow density of  $220 \frac{Kg}{m^3}$ . These results are shown in Figure 12.

The behavior shown in Figure 12 follows the logical expectation of how the avalanche would develop, considering the geometry of the slide path. In the early stages the velocity will increase rapidly. This will be followed by a leveling off and a slight decrease on the interval where the slope angle decreases. The avalanche's velocity then increases again as the terrain becomes steeper. The relation between the velocities also make logical sense. The deeper the entrainment and the denser the snow being entrained, the slower the avalanche will be able to move.

The density results in Figure 13 show the avalanche density is very sensitive to the the entrainment depth and snow density. For the 55cm weak layer, the density increases significantly throughout the slide. The accuracy of the model in this high density, high depth case may be poor because snow densities do not usually exceed  $500 \frac{Kg}{m^3}$  [2]. This drastic increase in density contrasts sharply with the 18cm entrainment slide. In the shallow slide, the density initially increases slightly but then decreases, ending at nearly the same density as the initial slide.

The volumes of the avalanches as seen in Figure 14 are also sensitive to the entrainment depth and snow density. The avalanche with shallower entrainment and less dense snow will have a greater increase in volume than the more dense, deeper slides. Initially this seems counter intuitive; however, when thought of in the context of a powder snow avalanche, the less dense snow will entrain more air causing its

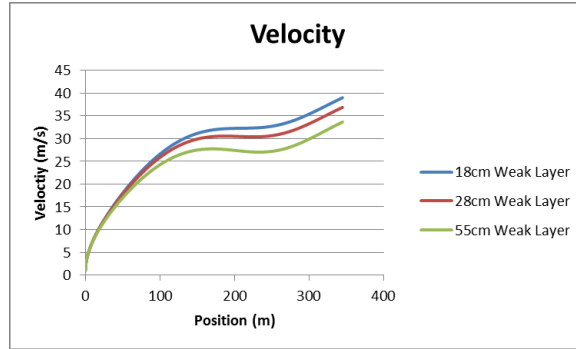


Figure 12: Velocity for Copper Bowls slide path for different erosion depths and densities at each depth. Green line 55cm erosion with 22% water density. Red Line 28cm erosion with 16% water. Blue line 18cm erosion depth with 11% water.

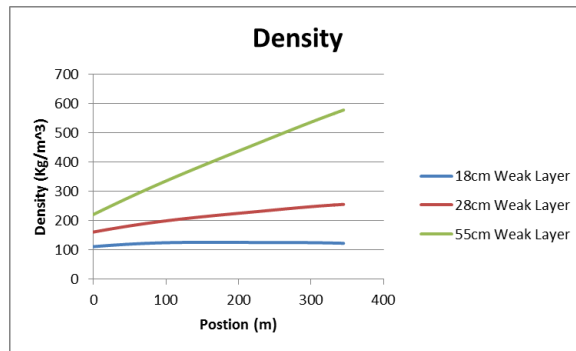


Figure 13: Density for Copper Bowls slide path for different erosion depths and densities at each depth. Green line 55cm erosion with 22% water density. Red Line 28cm erosion with 16% water. Blue line 18cm erosion depth with 11% water.

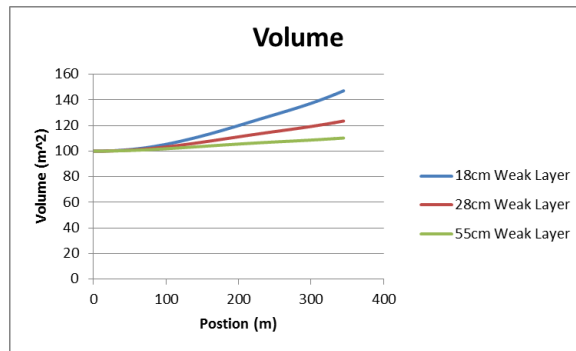


Figure 14: Volume for Copper Bowls slide path for different erosion depths and densities at each depth. Green line 55cm erosion with 22% water density. Red Line 28cm erosion with 16% water. Blue line 18cm erosion depth with 11% water.

volume to grow more than the denser slides.

For clarity, this can also be thought of in the same context as throwing a snowball.

If the snowball is densely packed, the volume will be near the same when it hits the ground. On the other hand, when throwing a snowball that is not tightly packed, as soon as it leaves your hand its volume greatly increases as it falls to the ground, just as the less dense avalanche grows in size.

## 9.4 Stonewall Results

One of the most popular backcountry ski locations in central Montana is the Stonewall Creek drainage, just outside of Lincoln, MT. For this slide path, we again used Google Earth. This gave us the data in Figure 15.

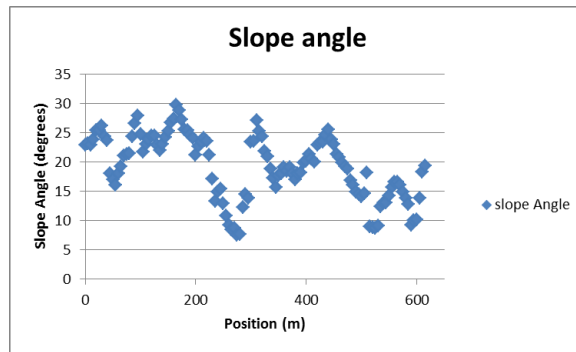


Figure 15: Slope angle vs. position for slide path in Stonewall creek drainage

Due to the complexity of this data, we could not find a function with an acceptable sum of the squares of the residuals. We then decided to use Euler’s Method with only the original data, instead of a function for slope angle. To help confirm we were not losing the integrity of the analysis, we used a step size of 5m for the Copper Bowls slide path and observed how the model changed. The results of this analysis are in Figure 16. Looking at these graphs in relation to those in Figures 9, 10, and 11, we lose some resolution especially in the early stages of the velocity graph, however, the long term behavior is the same. Due to the difficulty of reducing the step size of this complex data set, we decided the original data values with step size 5m were acceptable although not ideal.

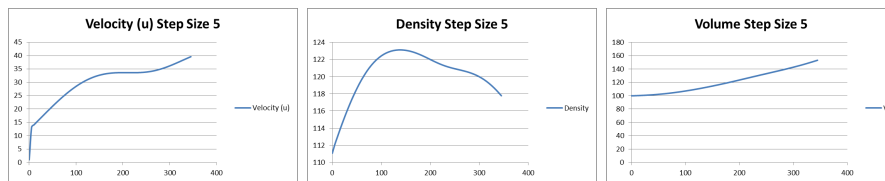


Figure 16: Graphs of Copper Bowls slide path using step size of 5m

The Stonewall slide path results are shown in Figures 17, 18, and 19. The velocities of the slides in the Stonewall slide path are slightly higher than those in the Copper

Bowls path. This could possibly be due to the length of the path. The density and volume graphs are qualitatively very similar to those of the Copper Bowls. However, in Figure 18 the density of the 55cm slide get well beyond the density snow can usually achieve. As discussed before, these unrealistic results point to a flaw in the model.

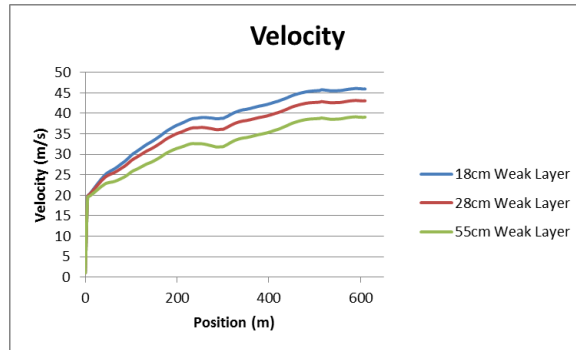


Figure 17: Velocity for Stonewall drainage slide path for different erosion depths and densities at each depth. Green line 55cm erosion with 22% water density. Red Line 28cm erosion with 16% water. Blue line 18cm erosion depth with 11% water.

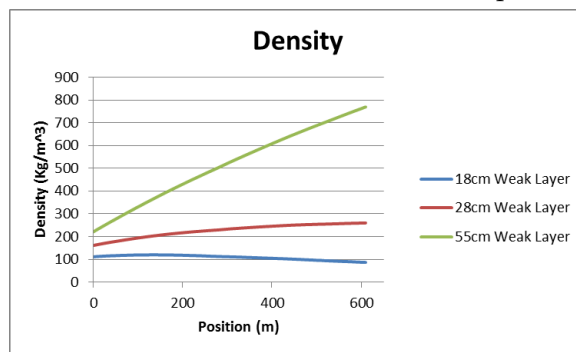


Figure 18: Density for Stonewall Drainage slide path for different erosion depths and densities at each depth. Green line 55cm erosion with 22% water density. Red Line 28cm erosion with 16% water. Blue line 18cm erosion depth with 11% water.

## 9.5 Morrell Results

One of the most popular backcountry ski locations in the Helena area is Morrell mountain in the southern Swan Range near Seeley Lake. Mapping a slide path in the same manner as the Copper Bowls slide path, we get the data in Figure 20. Similar to the Stonewall slide path, there is no simple function which would fit this data adequately. The lack of an acceptable function forced us to again only use the raw data, instead of a function, for slope angle. The results of this analysis are contained in Figures 21, 22, and 23. The velocities of the slides on this path are slightly higher than those on the Copper Bowls slide path. One possible reason for this is because there is no leveling out anywhere in this path. The densities and velocities for the Morrell slide path appear to be nearly identical to those of the Stonewall slide path.

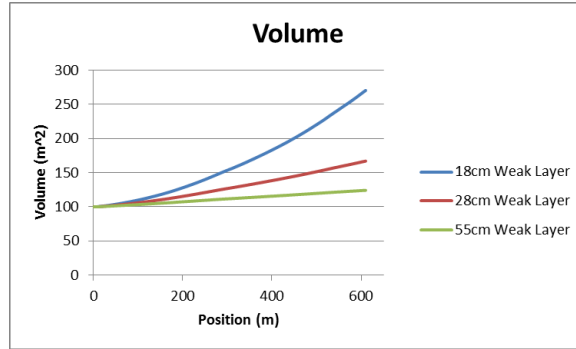


Figure 19: Volume for Stonewall drainage slide path for different erosion depths and densities at each depth. Green line 55cm erosion with 22% water density. Red Line 28cm erosion with 16% water. Blue line 18cm erosion depth with 11% water.

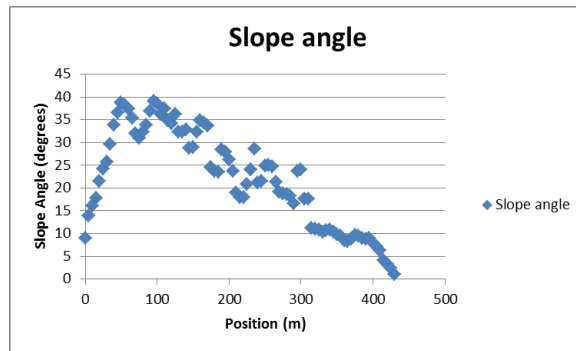


Figure 20: Slope angle vs. position for slide path on Morrell Mountain

The similarity of the densities and volumes of all three paths leads us to conclude that the density and volume in this model are not very sensitive to slope angle and are almost exclusively determined by entrainment depth and snow density.

## 10 Strengths and Weaknesses

According to Turnbull [4], the results of the velocities from the KSB model “match reasonably well the data gathered from avalanche 200 by Gruber [2004]” in the Vallée de la Sionne. The Vallée de la Sionne is a full scale avalanche test site in Switzerland. In the analysis done by Turnbull [4], the volume and densities also seem to reasonably match the observed data. However, it is also noted that for long slide paths, the densities do achieve unrealistically high values. The accuracy of the model when applied to the Vallée de la Sionne avalanche 200 allows us to predict the model’s accuracy for the Montana slide paths. Without observed data, however, there is no way to confirm the accuracy of the results. When considering our results as well as Turnbull [4] it becomes apparent that the the very large densities can be regarded as inaccurate. The densities for the 18cm and the 28cm entrainment depths seem

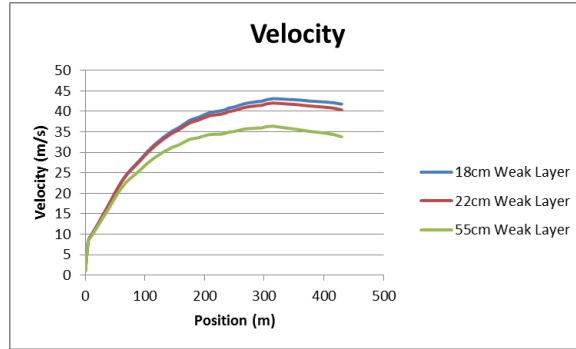


Figure 21: Velocity for Morrell Mountain slide path for different erosion depths and densities at each depth. Green line 55cm erosion with 22% water density. Red Line 28cm erosion with 16% water. Blue line 18cm erosion depth with 11% water.

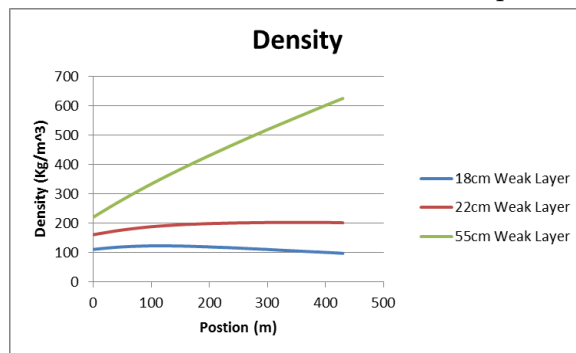


Figure 22: Density for Morrell Mountain slide path for different erosion depths and densities at each depth. Green line 55cm erosion with 22% water density. Red Line 28cm erosion with 16% water. Blue line 18cm erosion depth with 11% water.

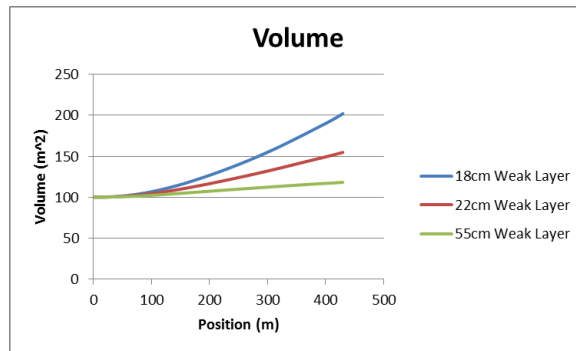


Figure 23: Volume for Morrell Mountain slide path for different erosion depths and densities at each depth. Green line 55cm erosion with 22% water density. Red Line 28cm erosion with 16% water. Blue line 18cm erosion depth with 11% water.

feasible, and with the information available, we see no reason to regard these as inaccurate. Due to the high variability of snow pack characteristics, the results from

any simulation cannot be used to estimate another similar slidepath unless they are geographically “close” and on the same aspect, e.g, south facing. Even though this is a significant downfall to the model, this is not unique to the KSB model and will present itself in any model dealing with snow conditions regardless of the sophistication.

## 11 Future Possibilities

Future work could result in the more accurate mapping of the slide paths because even though the data from Google Earth appeared accurate, significant differences would be possible in areas of heavy drifting and cornicing. This inaccuracy could greatly affect the starting zones of these avalanches.

A more in-depth review of how the snow entrainment process happens could be explored in order to avoid the unrealistically high densities in the later stages of the avalanches. A deeper understanding of the internal dynamics of avalanches could allow for an increased accuracy in the settling stage of the slide. This increased accuracy could also add significantly to the complexity of the model and detract from the beauty of the computational ease while maintaining fairly accurate results.

## 12 Conclusion

The KSB Model provides a fairly accurate depiction of a proposed avalanche while being computationally cheap. This allows the model to be adapted to many different slide paths without extensive changes being made to the model or taking a significant amount of additional time. Using the results of this model, we will be able to determine how serious an avalanche would be in these popular locations based on the current snow conditions.

## References

- [1] “avalanche.” *Dictionary.com Unabridged*. Random House, Inc. 14 Mar. 2013. Dictionary.com <http://dictionary.reference.com/browse/avalanche>.
- [2] “Welcome to California Cooperative Snow Surveys Website.” *California Cooperative Snow Surveys*. California Department of Water Resources, 2012. Web. 10 Mar. 2013. <http://cdec.water.ca.gov/snow/misc/density.html>
- [3] Google Inc. (2009). Google Earth (Version 5.1.3533.1731) [Software] Available at <http://www.google.com/earth/index.html>
- [4] Turnbull, B., J. N. McElwaine, and C. Ancey (2007), Kulikovskiy Sveshnikova Beghin model of powder snow avalanches: Development and application, *J. Geophys. Res.*, 112, F01004, doi:10.1029/2006JF000489.
- [5] Nate Woods, personal conversation, February 18, 2013.

[6] Dr. Kelly Cline, personal conversation, 2012, 2013.